Influence of non-ideal diffuse sound field excitations on the control performance of active panel structures

M. Misol [1], **C. Bloch** [1], **H. P. Monner** [1], **M. Sinapius** [1]
[1] German Aerospace Center, Institute of Composite Structures and Adaptive Systems, Braunschweig, Germany
e-mail: **malte.misol@dlr.de**

Abstract

The sound transmission loss of lightweight structures can be increased by the application of facing formworks. In the aircraft industry this task is accomplished by means of sidewall panels (linings) mounted on the primary fuselage structure of an aircraft. At low frequencies ($< 1000\,\mathrm{Hz}$), however, the sound transmission loss is dominated by the so-called mass-law which prescribes an inverse relationship between mass and transmitted sound power. This behavior is worsened by the fact that around the so-called mass-air-mass-resonance-frequency the transmission loss of a double panel structure (e.g., an aircraft fuselage structure with linings) falls below that of a single panel (of equal mass). Furthermore, the effectiveness of passive damping methods is limited due to constraints on mass and volume. On the other hand, the interior acoustics in the aircraft cabin is an important issue regarding passenger comfort, which raises the demand for alternative solutions. Active structural acoustic control (ASAC) provides a lightweight-compliant solution to the problem of low-frequency sound transmission through single or double panel structures. Prior to wind-tunnel or flight tests, the acoustic performance of active lightweight structures is usually tested in sound transmission loss facilities. A reverberation room, equipped with one or a number of independent sound sources, is used to generate a diffuse sound field excitation. Although it is well-known that the statistical properties of such a non-ideal diffuse sound field will deviate from the ideal case, potential implications on the performance of active feedforward control systems have not been discussed so far. This is why this work evaluates the spatial coherence of ideal and non-ideal diffuse sound fields and considers the implications on feedforward control performance. The system under consideration is an aircraft-typical double panel system, equipped with an active sidewall panel, which is realized in a transmission loss facility. Experimental results for different numbers of sound sources in the reverberation room are compared to simulation results of a generic double panel system excited by an ideal diffuse sound field. It is shown that the number of statistically independent noise sources acting on the primary structure depends not only on the type of diffuse sound field but also on the sample lengths of the processed signals. The experimental results show that the number of reference sensors required for a defined control performance has an inverse relationship to the control filter length.

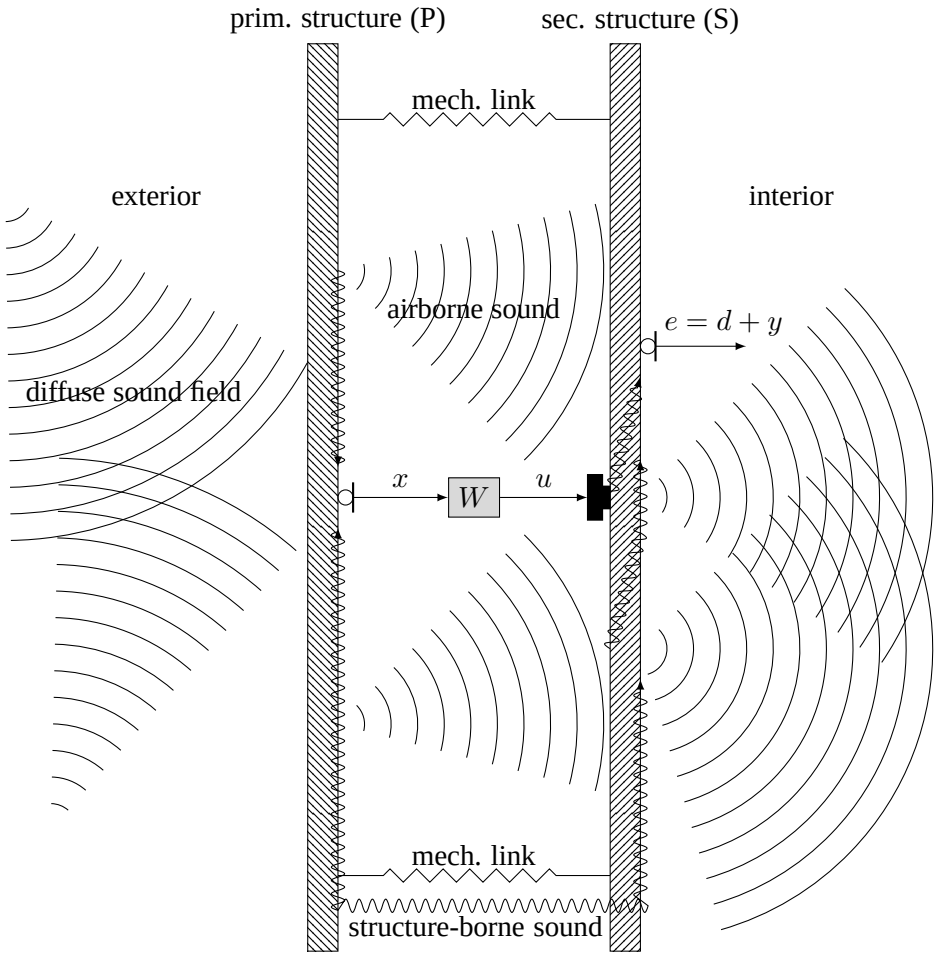

Figure 1: Principle of the active feedforward control of sound transmission through a double panel system.

1 Introduction

The limited sound transmission loss of lightweight structures, such as aircraft sidewall panels, at low frequencies is an important issue regarding passenger comfort. Active structural acoustic control (ASAC) provides a lightweight-compliant solution to the problem of low-frequency sound transmission through single or double panel structures. The experimental performance evaluation of such systems is usually done in a sound transmission loss facility with a reverberant sending room. A diffuse sound field, which is synthesized in this room, serves as the disturbance excitation of the structural system under consideration. Although it is known that the statistical properties of the synthesised diffuse sound field will deviate from the ideal case, potential implications on the performance of active feedforward control systems have never been discussed. One reason for this might be the fact that the active control of stochastic disturbance excitations is usually considered as a domain of feedback algorithms. However, if coherent and sufficiently time-advanced reference signals are available, the application of feedforward control is not limited to deterministic disturbances. This was experimentally verified by the authors [15, 16] using the example of an aircraft-typical double panel system, where the reference sensors are placed on the primary fuselage structure and the actuators and error sensors are located on the secondary sidewall panel structure. A principle drawing of such a configuration is provided in Figure 1. It can be seen, that the primary structure (P), which is excited by a diffuse sound field, acts as the disturbance source for the secondary structure (S). The primary disturbance propagates via structure-borne and airborne sound to S which starts to vibrate and to radiate sound into the interior. An active feedforward control system (control filter W) is realized by the application of reference sensors (reference signals x) on P and actuators and error sensors (error signals e) on S. It is central to this paper, that the required number of

reference sensors on P (in order to achieve a sufficiently high coherence) is heavily influenced by the spatial coherence of the diffuse sound field. The same experimental system as in Misol et al. [15] is applied here in order to evaluate the implications of non-ideal diffuse sound fields on the performance of active feedforward-controlled structures. The research work was triggered by the observation that the number of independent components observed in the reverberation room's pressure field or likewise in the vibration response of a structure depends on the analysis-window-size or the frequency resolution, respectively. The implications on the control performance are due to the fact that the frequency resolution of a feedforward controller depends on the number of filter weights, which is a free parameter in control design.

Regarding the topic of diffuse sound fields and their generation in reverberation rooms, much theoretical and experimental research work has been published. According to Jacobsen and Roisin [12], the ideal diffuse sound field is defined as "[...] a sound field in an unbounded medium generated by distant, uncorrelated sources of random noise evenly distributed over all directions". Following the definition of Elliott et al. [5], a diffuse sound field is induced by a superposition of an infinite number of uncorrelated plane waves. Due to the absence of interferences, the ideal diffuse sound field is homogeneous and isotropic. Regarding the practical realisation of diffuse sound fields in reverberation rooms, the spatial correlation or the Schröder frequency [19] are frequently used as indicators or conditions for the quality of the synthesised pressure field. Yet, the spatial coherence, which describes the number of independent components, is rarely considered in this context and has never been linked with the realisation of active systems or structures. As already mentioned, most of the published research work focusses on the design and implementation of active single or double panel systems which are controlled by feedback algorithms. Past and recent work in this field has been published for example by Gardonio and Elliott [10], Engels et al. [6] or Gardonio and Alujevic [8]. Similar questions with special emphasis on the evaluation of different actuation principles are addressed in Bao and Pan [2, 17] or in Gardonio and Elliott [9]. In the authors' opinion, not much research work has been published concerning the practical implementation of active structures in sound transmission loss facilities, and even fewer publications are concerned with the active feedforward control of stochastic structural vibration and the experimental evaluation of smart structures under realistic conditions.

The main body of the paper is divided into three sections. Section 2 starts with a theoretical discussion of the spatial coherence properties of an ideal diffuse sound field. Subsequently, the modeling and simulation of an ideal (pure-tone) and the synthesis of a real non-ideal diffuse sound field is described. The section ends with the evaluation of the spatial coherence of the ideal and non-ideal diffuse sound fields.

Section 3 focusses on the active feedforward control of broadband and spatially weakly correlated disturbances. Firstly, the influence of coherence on the feedforward control performance is discussed. Subsequently, a connection between the statistical parameters of the diffuse sound field excitation and the coherence between the reference and the disturbance signals of the active feedforward control system is established. The virtual noise source theory establishes the link between the two topics of this paper: the statistical properties of the diffuse sound field and the performance of the feedforward control system. The section ends with a brief description of the optimal causal feedforward controller used in this work.

Section 4 documents the numerical and experimental investigation of the double panel system. It starts with a brief description of the experimental setup and the simulation model. Subsequently, the methodology used for the derivation of the analysis results is described. Finally, the numerical and experimental data is evaluated regarding the relative strength of the virtual noise sources and the relative control performance of different feedforward control system configurations.

2 Diffuse sound field

2.1 Theoretical background

The spatial coherence of a diffuse sound field is evaluated using the mean squared coherence $|\gamma_{xy}|^2$ of two sound pressure signals x and y, measured in a diffuse sound field at a distance r.

$$|\gamma_{xy}(\omega)|^2 = \frac{|S_{xy}(\omega)|^2}{S_{xx}(\omega)S_{yy}(\omega)} \tag{1}$$

The cross-power spectral density is denoted by S_{xy} and the power spectral densities by S_{xx} and S_{yy}, respectively. According to Elliott et al. [5], the cross-power spectral density of the pressures at two points in an ideal diffuse sound field is given by Equation (2).

$$S_{xy}(\omega, r) = S_{pp}(\omega)\frac{\sin(kr)}{kr} \tag{2}$$

Since the diffuse sound field is assumed to be ideal, the power spectral density S_{pp} of the sound pressure is independent of position. This leads to an expression for the spatial coherence of an ideal diffuse sound field given in Equation (3).

$$|\gamma_{xy}(\omega, r)|^2 = \frac{|S_{xy}(\omega, r)|^2}{S_{pp}^2(\omega)} = \left(\frac{\sin(kr)}{kr}\right)^2 \tag{3}$$

The validity of Equation (3) is discussed in Jacobsen and Roisin [12]. In Elliott et al. [5] it is mentioned that the sound field in a reverberation room can be considered as being diffuse, provided that the excitation frequencies are higher than the room's Schröder frequency. However, the spatial coherence of an ideal diffuse sound field will only be approximated well if the number of uncorrelated sound sources in the reverberation room is high enough. This condition is normally violated in reverberation rooms because of hardware limitations. Since the spatial coherence of the disturbance excitation is crucial for the design and the performance of an active structural acoustic control system with feedforward control law, it will be analysed subsequently by means of a pure-tone diffuse sound field simulation model and by means of measurement data captured in a reverberation room.

2.2 Modeling and Simulation

Following the definition of Elliott et al. [5], a diffuse sound field can be modelled by superposing a multitude of plane acoustic waves with random phase angles incident from all directions. The synthesis of the required plane waves is accomplished by means of acoustic point sources with stochastic phase angles that are evenly distributed on a half-sphere of sufficiently large dimension. In this study, a total of 300 acoustic monopoles are evenly distributed on a half-sphere with a radius of $100\,\mathrm{m}$. The mathematical expression for the sound pressure of an acoustic monopole is taken from Fahy and Gardonio [7, p. 139]. The superposed complex pressure amplitudes induced by the acoustic monopoles are evaluated on the measurement grid in order to obtain the complex diffuse sound field pressure amplitudes. However, according to Jacobsen and Roisin [12] the described method equals a pure-tone model resulting in interferences of the plane waves. Since the pure-tone model deviates from the ideal, homogeneous and isotropic diffuse sound field model, its characteristics are calculated and compared to the ideal case.

2.3 Synthesis in a reverberation room

Real diffuse sound fields are generated in reverberation rooms excited by at least one or a few statistically independent sound sources. In this study, a reverberation room of $\approx 200\,\mathrm{m}^3$ with a mean reverberation time $\bar{T}_{60} \approx 5\ s$ (averaged over third-octave bands from $80\,\mathrm{Hz}$–$5000\,\mathrm{Hz}$) was used. The room fulfills the ISO 3741 standard (accuracy class 1) for frequencies above $100\,\mathrm{Hz}$. The excitation of the reverberation room was realised by means of either an omnidirectional dodecahedron sound source with twelve shunted electrodynamic loudspeakers (all excited by the same signal) or of ten independent electrodynamic loudspeakers, which are

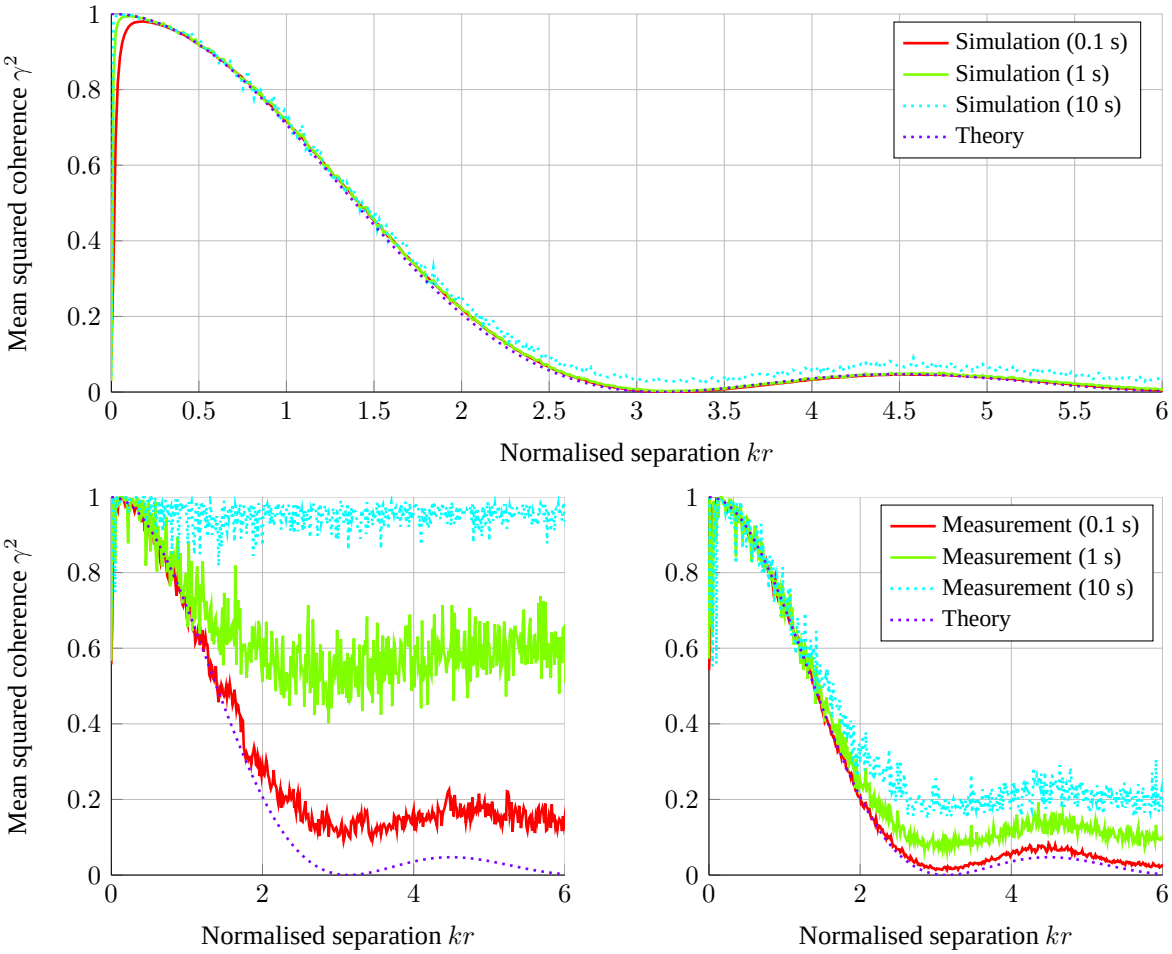

Figure 2: Spatial coherence of the simulated diffuse sound field (top) and the real diffuse sound field synthesized with either one sound source (bottom left) or with ten independent sound sources (bottom right) in dependency of the normalized separation kr.

part of a loudspeaker array. The dodecahedron sound source was driven by a bandlimited white noise signal with a frequency range of 0 Hz–5000 Hz, the loudspeaker array by ten uncorrelated, bandlimited white noises ranging from 80 Hz–5000 Hz. The sound pressure was measured using $1/4$" ICP® microphones of the type PCB 130D21.

2.4 Evaluation of spatial coherence

Figure 2 (top) shows the spatial coherence of the simulated diffuse sound field as a function of the normalised separation kr. Apparently, the applied pure-tone diffuse sound field model approximates the spatial coherence properties of an ideal diffuse sound field to a very high accuracy. The slight deviations between the theoretical and the simulated mean squared coherence for a sample length of $10\ s$ are attributed to the lesser amount of periodograms available for the calculation of the expected values (by temporal averaging). Hence, the pure-tone diffuse sound field simulation model can be applied as an ideal excitation model for the simulation-based design of active feedforward-controlled structures. The spatial coherences of the real diffuse sound fields are provided in the lower parts of Figure 2. Figure 2 (bottom left) shows the spatial coherence of the diffuse sound field excited by a single sound source as a function of the normalised separation kr. Apparently the deviation between real and theoretical coherence rises with increasing sample length (from 0.1 s to 10 s). This behavior is explained by the fact that the reverberation room acts as an acoustic energy storage. If the excitation is stochastic, a short sequence of sound pressure signals (sample

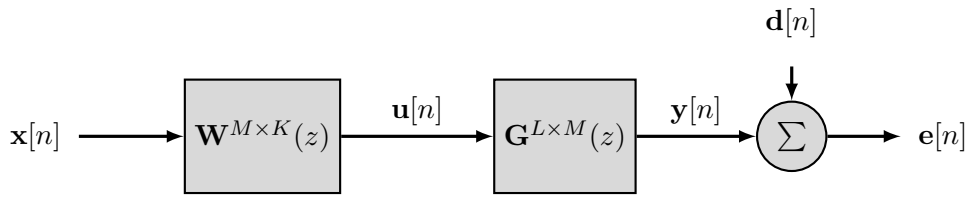

Figure 3: Block diagram of an active feedforward control system with K reference sensors, M actuators and L error sensors.

length $\ll T_{60}$) contains a large amount of uncorrelated sound energy. Since the amount of stored energy is proportional to the reverberation time, the influence of uncorrelated components decreases for larger sample lengths. As a consequence, the spatial coherence rises with increasing sample length. Jacobsen and Roisin [12] provide an alternative explanation based on the bandwidth of the excitation signal and the characteristic dimension of the reverberation room. Figure 2 (bottom right) shows the spatial coherence of the diffuse sound field excited by ten uncorrelated sound sources as a function of the normalised separation kr. The existence of multiple uncorrelated sound sources in the reverberation room leads to a higher correspondence between the theoretical and the real diffuse sound field. However, the coherence of the real diffuse sound field rises for increasing sample lengths which indicates that the theoretical number of independent sources of an ideal diffuse sound field has still not been reached. More information regarding the statistical properties of the investigated diffuse sound fields can be found in Misol et al. [14].

3 Active feedforward control

Figure 3 shows the general scheme of a feedforward control system. The control signals $\mathbf{u}$ are generated by filtering the reference signals $\mathbf{x}$ through the control filter $\mathbf{W}$. The secondary path $\mathbf{G}$ describes the whole dynamics and delays (except the contribution of $\mathbf{W}$) between the reference and the error sensors. This includes the delays introduced by analog and digital signal processing (DSP). The error signal $\mathbf{e}$ is the sum of the filtered control signals $\mathbf{y}$ and the disturbance signals $\mathbf{d}$. A comparison with Figure 1 clarifies the physical significance of the block diagram provided in Figure 3.

3.1 Coherence

The performance of an active feedforward controller is largely influenced by the availability of time-advanced and coherent reference signals. The first requirement is related to the causality of the feedforward control system. For broadband excitations like a diffuse sound field, the causality constraint is an important issue. Yet, this work focusses on the second requirement, as the implications of non-ideal diffuse sound fields on the coherence and the performance of a feedforward control system are crucial.

A connection between control performance and coherence is provided by Minkoff [13] for the special case of a system with $K \equiv M \equiv L \equiv 2$. For reasons of clarity, no virtual transfer functions are defined between reference and disturbance signals, as had been the case in the formula provided by Minkoff. Therefore, the cost function described in Equations (4) and (5) slightly differs from the original one.

Under the assumption that the feedforward controller does not increase the value of the cost function, the third summand of Equation (5) has to be positive. Consequently, J_{min} will reach its minimum if the mutual coherence between the reference signals $|\gamma_{x_1x_2}|^2$ (and with it $S_{x_1x_2}$) vanishes and the multiple coherence between the disturbance and the reference signals $|\gamma_{d_i\mathbf{x}}|^2$ is equal to one. However, due to the spatial correlation of the sound pressure in a diffuse sound field and because of the filtering effect of the structural system, the reference signals are not statistically independent. Hence the mutual coherence will generally be greater than zero. Furthermore, for higher frequencies and under the restriction of a limited number of

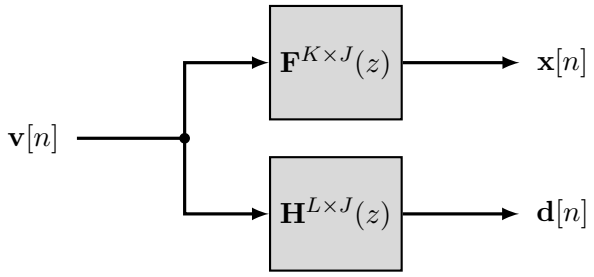

Figure 4: Synthesis of reference signals $\mathbf{x}$ and disturbance signals $\mathbf{d}$ from virtual noise sources $\mathbf{v}$.

reference sensors, not the whole disturbance source information will be captured, which results in a drop of the multiple coherence. According to Equation (5) both effects will lead to an increase of J_{min} and with that to a deterioration of the disturbance rejection of the active feedforward control system. Further insight into the connection between the statistical properties of the excitation and the feedforward control performance is gained by applying the virtual noise source theory.

$$
\begin{aligned}
J_{min} &= S_{d_1d_1}\left(1-\frac{|\gamma_{d_1x_1}|^2+|\gamma_{d_1x_2}|^2}{1-|\gamma_{x_1x_2}|^2}\right)+2\ \mathrm{Re}\left[\frac{S_{x_1x_2}}{S_{x_1x_1}S_{x_2x_2}}\frac{S_{x_1d_1}S^*_{x_1d_2}}{1-|\gamma_{x_1x_2}|^2}\right]\dots \qquad (4)\\
&+ S_{d_2d_2}\left(1-\frac{|\gamma_{d_2x_2}|^2+|\gamma_{d_2x_1}|^2}{1-|\gamma_{x_1x_2}|^2}\right)+2\ \mathrm{Re}\left[\frac{S_{x_1x_2}}{S_{x_1x_1}S_{x_2x_2}}\frac{S_{x_2d_1}S^*_{x_2d_2}}{1-|\gamma_{x_1x_2}|^2}\right]\\
&= S_{d_1d_1}+S_{d_2d_2}-\frac{1}{1-|\gamma_{x_1x_2}|^2}\{S_{d_1d_1}\left(|\gamma_{d_1x_1}|^2+|\gamma_{d_1x_2}|^2\right)\dots \qquad (5)\\
&- 2\ \mathrm{Re}\left[\frac{S_{x_1x_2}S_{x_1d_1}S^*_{x_1d_2}}{S_{x_1x_1}S_{x_2x_2}}\right]+S_{d_2d_2}\left(|\gamma_{d_2x_2}|^2+|\gamma_{d_2x_1}|^2\right)-2\ \mathrm{Re}\left[\frac{S_{x_1x_2}S_{x_2d_1}S^*_{x_2d_2}}{S_{x_1x_1}S_{x_2x_2}}\right]\}
\end{aligned}
$$

3.2 Virtual noise source theory

The concept of virtual noise sources described in Akiho et al. [1] provides a method to identify the number of statistically independent components in a sound or vibration field. In Elliott et al [5], this method is used to calculate the density of uncorrelated components in an ideal diffuse sound field. In this study, the theory is applied to structural reference signals measured on the primary structure P of a double panel system excited by a diffuse sound field (see Figure 1). The number of independent components in the vibration field of P, which act as disturbance sources of the secondary structure S, corresponds to the number of non-zero eigenvalues of the power spectral density matrix

$$\mathbf{S_{xx}} = \mathbb{E}\left[\mathbf{X}\,\mathbf{X}^H\right]\ . \qquad (6)$$

The expectation $\mathbb{E}$ is realized by averaging a sufficient number of periodograms (time averaging of stationary and ergodic signals). Whether or not an eigenvalue must be considered as dominant, depends on the prescribed control performance. In order to impose a tolerance limit on the eigenvalues, their physical meaning and influence on the multiple coherence of the disturbance and the reference signals has to be assessed.

Figure 4 shows the connection between the virtual noise sources $\mathbf{v}$, the reference signals $\mathbf{x}$ and the disturbance signals $\mathbf{d}$. Accordingly, the power spectral density matrix of Equation (6) can be rewritten as

$$\mathbf{S_{xx}} = \mathbb{E}\left[\mathbf{X}\,\mathbf{X}^H\right] = \mathbb{E}\left[\mathbf{F}\mathbf{V}\,\mathbf{V}^H\mathbf{F}^H\right] = \mathbf{F}\,\underbrace{\mathbb{E}\left[\mathbf{V}\,\mathbf{V}^H\right]}_{\mathbf{S_{vv}}=\Sigma}\,\mathbf{F}^H\ . \qquad (7)$$

Since the virtual noise sources are uncorrelated, Equation (7) takes the form of an eigenvector/eigenvalue decomposition. The matrix $\mathbf{F}$ contains the eigenvectors and the diagonal matrix Σ contains the eigenvalues of $\mathbf{S_{xx}}$. It follows, that the eigenvalues $\sigma_i = \Sigma_{ii}$ of $\mathbf{S_{xx}}$ are equal to the power spectral densities $\mathbb{E}\left[v_i v_i^*\right]$ of the virtual noise sources. Assuming that the magnitudes of the frequency response functions (FRF) $H_{ij} = H_{d_i v_j}$ with $i = 1, ..., L$ are identical or at least similar for all j, the relative contribution of a virtual noise source v_j to the disturbance signal's PSD $|D_i|^2$ at error sensor i equals the eigenvalue σ_j. This follows from

$$\mathbf{S_{dd}} = \mathbb{E}\left[\mathbf{D}\,\mathbf{D}^H\right] = \mathbb{E}\left[\mathbf{H}\mathbf{V}\,\mathbf{V}^H\mathbf{H}^H\right] = \mathbf{H}\,\Sigma\,\mathbf{H}^H = \sum_{j=1}^{J} \mathbf{H}_j \mathbf{H}_j^H \sigma_j \tag{8}$$

and

$$\mathrm{tr}\left(\mathbf{S_{dd}}\right) = \sum_{i=1}^{L}\sum_{j=1}^{J} |H_{ij}|^2\,\sigma_j \xrightarrow{|H_{ij}|=|H_i|} \sum_{i=1}^{L} |H_i|^2\left(\sigma_1 + \sigma_2 + \cdots + \sigma_J\right) = \sum_{i=1}^{L} |D_i|^2\,. \tag{9}$$

Hence, capturing the largest $N \leq J$ virtual noise sources $\mathbf{v}_N = [v_1, v_2, \ldots, v_N]$ by means of $K = N$ optimally or $K > N$ suboptimally placed reference sensors facilitates a multiple coherence of reference and disturbance signals of

$$\begin{aligned} C_{\mathbf{x}d_i} = C_{\mathbf{v}_N d_i} &= \frac{\mathbf{S}_{\mathbf{v}_N d_i}\Sigma^{-1}\mathbf{S}_{\mathbf{v}_N d_i}^H}{S_{d_i d_i}} \\ &= \frac{|H_i|^2}{|H_i|^2\sum_{j=1}^{J}\sigma_j} \begin{bmatrix} \sigma_1 & \cdots & \sigma_N \end{bmatrix} \begin{bmatrix} \sigma_1^{-1} & \cdots & 0 \\ \vdots & \ddots & \vdots \\ 0 & \cdots & \sigma_N^{-1} \end{bmatrix} \begin{bmatrix} \sigma_1 \\ \vdots \\ \sigma_N \end{bmatrix} = \frac{\sum_{j=1}^{N}\sigma_j}{\sum_{j=1}^{J}\sigma_j}\,. \end{aligned} \tag{10}$$

The derivation of Equation (10) makes use of the linear relationship between x and $\mathbf{v}_N$ and exploits the mutual statistical independence of the virtual noise sources. The quotient of the error signal's and the disturbance signal's PSD

$$\frac{S_{e_i e_i}}{S_{d_i d_i}} = 1 - C_{\mathbf{x}d_i} = \frac{\sum_{j=N+1}^{J}\sigma_j}{\sum_{j=1}^{J}\sigma_j} < \frac{\sigma_{N+1}}{\sigma_1} \tag{11}$$

leads to an expression of the disturbance rejection at error sensor i

$$10\log_{10}\left(\frac{S_{e_i e_i}}{S_{d_i d_i}}\right) = 10\log_{10}\left(\frac{\sum_{j=N+1}^{J}\sigma_j}{\sum_{j=1}^{J}\sigma_j}\right) < 10\log_{10}\left(\sigma_{N+1}\right) - 10\log_{10}\left(\sigma_1\right)\ \mathrm{dB}\,. \tag{12}$$

Equation (12) provides a conservative estimate of the disturbance rejection of an active (causal) feedforward control system based on the eigenvalues of $\mathbf{S_{xx}}$. As already noted, not the absolute value of the eigenvalue level but the level difference is decisive for the disturbance rejection.

3.3 Optimal causal feedforward control

The calculation of the FIR-filter weights of the optimal causal feedforward controller is based on a matrix formulation for the error vector which permits an explicit expression for the vector of optimal filter coefficients. Details regarding the derivation of the FIR-filter weights can be found in Elliott [4, p. 237ff.]. The benefits of this method are its inherent causality, the specification of the number of filter weights and the

Device	Type	Other
Accelerometer	PCB® 352A24	$0,8\,\mathrm{g}$, $10,2\,{}^{\mathrm{mV}}/_{\mathrm{m/s^2}}$
Exciter (inertial)	VISATON® EX 45 S	$10\,\mathrm{W}$, $8\,\Omega$, $0,06\,\mathrm{kg}$
Lowpass filter	KEMO® CardMaster 255G	$f_c = 480\,\mathrm{Hz}$, $24\,{}^{\mathrm{dB}}/_{\mathrm{Oct.}}$
Real-time-system	DSPACE® DS1006	$F_s = 1000\,\mathrm{Hz}$

Table 1: Hardware components and settings of the active feedforward control system.

possibility to include control effort into the performance metric. According to Elliott [4, p. 249], the vector of optimal FIR filter weights is given by

$$\mathbf{w}_{opt} = -\left(\mathbf{R}_{\tilde{\mathbf{x}}\tilde{\mathbf{x}}} + \beta\mathbf{I}\right)^{-1}\mathbf{R}_{\tilde{\mathbf{x}}\mathbf{d}}\,. \tag{13}$$

The calculation of the auto-correlation matrix $\mathbf{R}_{\tilde{\mathbf{x}}\tilde{\mathbf{x}}}$ of the filtered reference signals $\tilde{\mathbf{x}}$ and the cross-correlation vector $\mathbf{R}_{\tilde{\mathbf{x}}\mathbf{d}}$ is performed in the frequency domain. Due to its block-Toeplitz structure, the auto-correlation matrix is highly redundant and iterative methods are available to solve for the optimal filter weights [18]. The regularisation factor $\beta \geq 0$ penalises the control effort and improves the numerical stability and robustness of the controller.

4 Double panel system

4.1 System

In this work, an active feedforward control system is implemented on an aircraft-typical double panel system. As shown in Figure 5, the system consists of a curved and stiffened carbon-fiber-reinforced plastics (CFRP) fuselage structure and three off-the-shelf aircraft sidewall spacer panels (linings). It must be noted that only the lining located in the middle is used for the active system (see Figure 6). The fuselage structure (P) is augmented with ten reference accelerometers R_1 to R_{10}, which measure the structural vibration induced by the diffuse sound field. Two collocated and dual pairs of error sensors E_i (accelerometers) and actuators A_i (inertial mass exciters) are used, which are mounted on the lining (S). Each actuator is applied collocated to the corresponding error sensor on the backside of the lining. This minimises the delay in the secondary paths G_{ii} with $i = 1, 2$ and thus increases the causality margin of the feedforward control system [15]. The hardware components and their setting are listed in Table 1. Figure 6 shows the interconnection of the sensors and the actuators via the analog and digital signal processing. For the system under consideration $K = 10$, $M = 2$ and $L = 2$. The analog low-pass filters are denoted by LP.

The simulations are carried out for a simplified, generic double panel system consisting of two flat panels coupled by an enclosed fluid. The structural coupling between the primary and the secondary structures is neglected, since, at low frequencies, the acoustic path dominates and "there exists an almost linear relation between the [...] acoustic potential energy in the cavity and the [...] radiated sound power" [3]. The geometrical and material properties of the generic system are similar to the real system, yet the horizontal width of P is limited to $0.5\,\mathrm{m}$ and thus equals the distance between two frames. This is according to Haase et al. [11] justifiable since the transmission of structure borne sound across ribs can be neglected. Further details on the modeling of the generic double panel system can be found in Misol and Hesse [16].

4.2 Methodology

The numerical and experimental results provided in the following are intended to clarify the relationship between the number of virtual noise sources and the performance of optimal causal feedforward control. The results of the analysis are provided by means of two different plot-types.

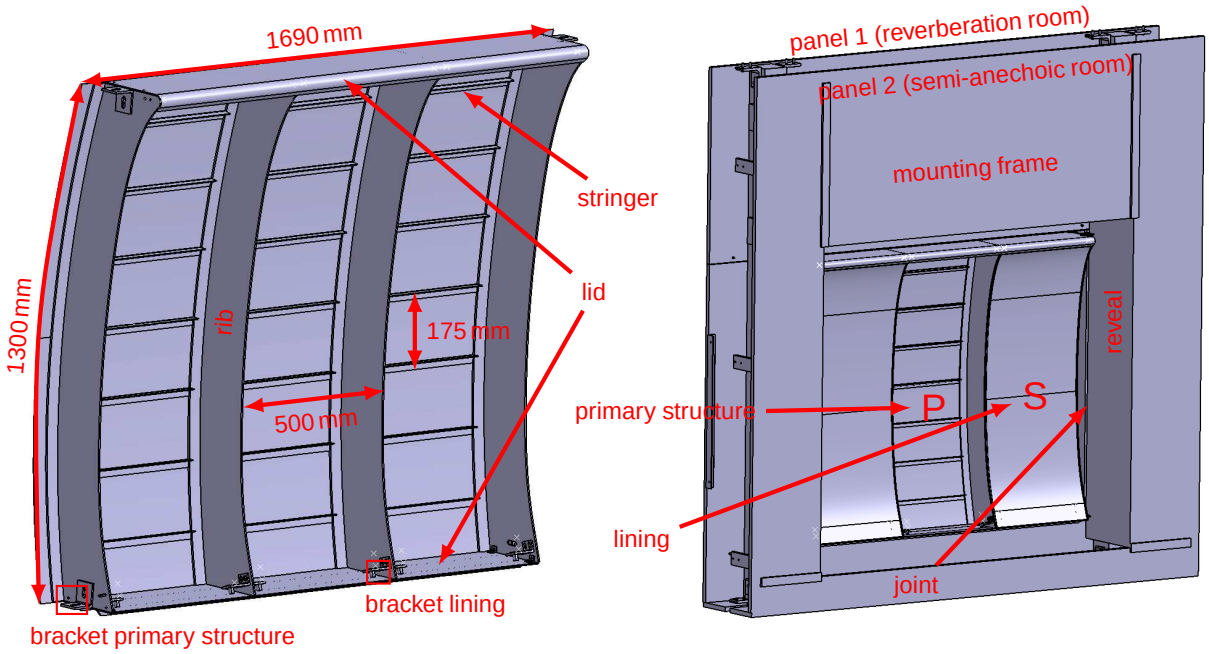

Figure 5: Design drawing of the CFRP-panel (left) and of the double panel system with mounting frame (right) seen from the semi-anechoic room of the transmission loss facility.

Firstly, in Figure 7, a contour plot of the eigenvalues of the power spectral density matrix $\mathbf{S_{xx}}$ is used in order to evaluate the strength of the virtual noise sources. It was shown in subsection 3.2 that the power spectral densities of the virtual noise sources are identical to the eigenvalues of $\mathbf{S_{xx}}$.

Secondly, in Figure 8, the disturbance rejection of a long FIR filter with 3000 filter taps is compared to that of a short FIR filter with 200 filter taps. It is assumed from subsection 2.4, that the FIR filter length will strongly influence the performance of the feedforward control system, since it determines the duration over which the filter correlates. The relative disturbance rejection $\Delta_{3000-200}$ is defined as the difference in the average third-octave band power level reduction of the short and of the long control filter (from 80 Hz–500 Hz). Different reference sensor configurations are considered in order to observe the interdependencies between control performance, FIR filter length, number of reference sensors and type of diffuse sound field excitation. It must be noted, that the FIR filter sizes correspond to the sample lengths of the analysis windows used for the calculation of the power spectral density matrix $\mathbf{S_{xx}}$. The configuration with 2 references uses R_3 and R_6, the configuration with 4 references uses R_1, R_4, R_6 and R_9 and the configuration with 7 references uses R_1, R_2, R_3, R_5, R_6, R_7 and R_{10}.

Further details on the synthesis of the measurement and simulation data can be found in Misol et al. [14].

4.3 Virtual noise sources

The magnitude of the contour plots in Figure 7 corresponds to the normalised eigenvalue levels $\lambda_i = 10\log_{10}(\sigma_i/\sigma_{max})$ dB. The spacing of the contour lines is 10 dB. If the required disturbance rejection amounts to 20 dB then – according to Equation (12) – the number of reference sensors K should be chosen such that $\lambda_1 - \lambda_{K+1} > 20\,\mathrm{dB}$. Two different analysis-window-sizes are chosen, one well below and one in the range of the reverberation time of the applied reverberation room. As is known from subsection 2.4, the sample length has a significant influence on the spatial coherence and thus influences the number of dominant virtual noise sources.

According to Figure 7 (top), the dependency of the eigenvalue levels on sample length is very weak. This result is in accordance with the spatial coherence shown in Figure 2 (top), which was only slightly increased

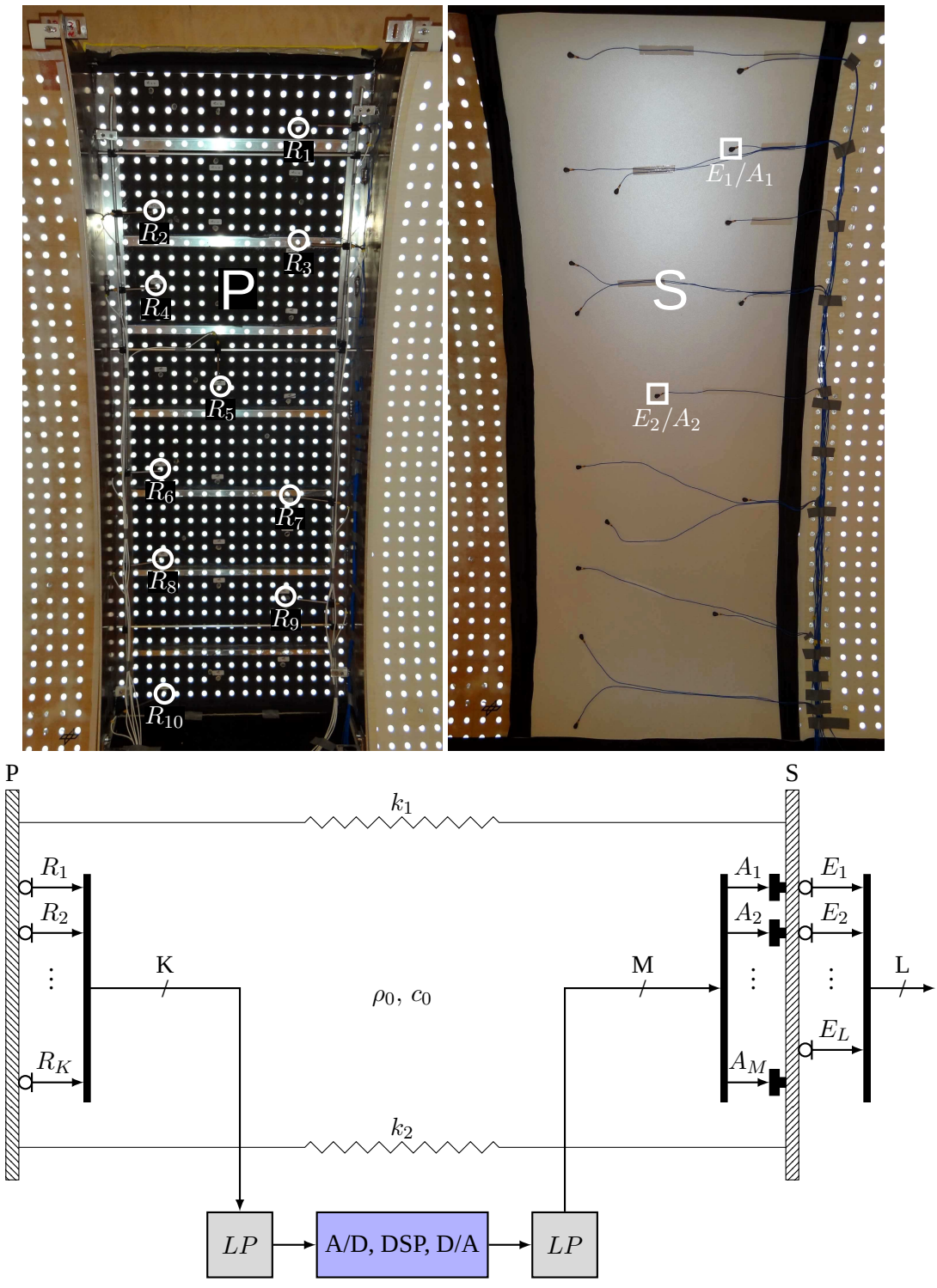

Figure 6: Active section of the double panel system with reference sensors (R_i) on the primary structure (top left) and error sensors (E_i) and actuators (A_i) on the secondary structure (top right). Interconnection of the active components with the real-time-system (bottom).

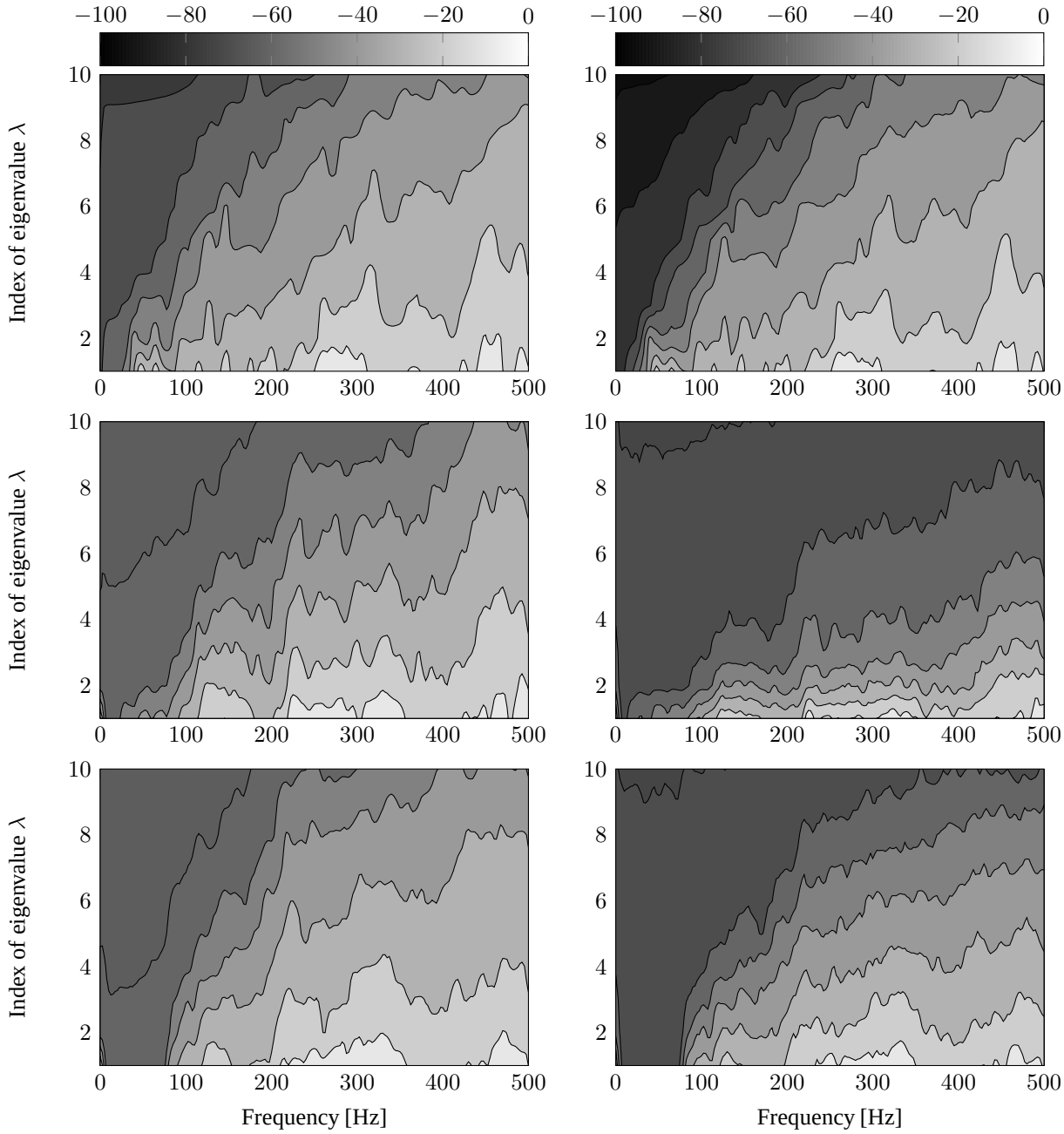

Figure 7: Normalized eigenvalue levels of the power spectral density matrix $\mathbf{S_{xx}}$ of the simulated (top) and the measured (middle and bottom) reference signals (from ten accelerometers) calculated with an analysis window of $0.4\,\mathrm{s}$ (left) and $6\,\mathrm{s}$ (right). Measurement results are shown for the diffuse sound field synthesized with a single sound source (middle) and with ten independent sound sources (bottom) in the reverberation room.

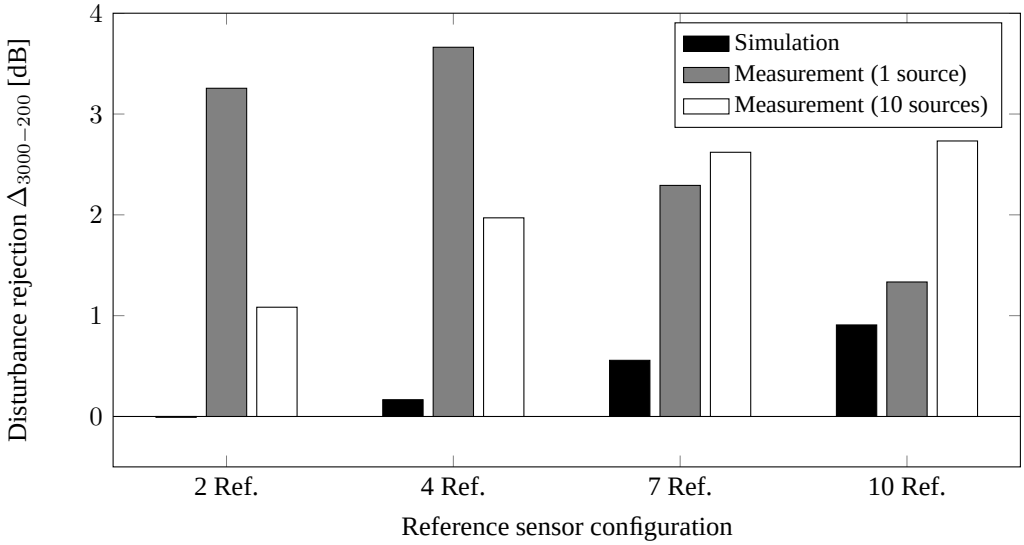

Figure 8: Difference in the disturbance rejection of a feedforward controller with 3000 and with 200 FIR-filter weights depending on the number of reference sensors and the type of the diffuse sound field.

for larger analysis windows. Figure 7 (top) further shows that the eigenvalue levels increase with frequency, which according to Elliott et al. [5] is typical for an ideal diffuse sound field. The monotonicity of the contour lines prescribed by the diffuse sound field is disturbed due to the influence of the structural dynamics of the double panel system. It follows from Figure 7 (middle), that the dependency of the eigenvalue levels on sample length for a non-ideal diffuse sound field with a single sound source in the reverberation room is much stronger compared to the previous case. Again, this behavior is in accordance with the spatial coherence shown in Figure 2 (bottom left), which converges to the theoretical value of the ideal diffuse sound field for very small analysis windows and which tends to one for the opposite case. It is thus assumed that a feedforward controller with short FIR filters will observe an almost ideal diffuse-sound-field-excitation and hence will require much more reference sensors as a feedforward controller with long FIR filters that correlates over a larger time span. The correctness of this assumption will be proven in the following subsection by means of the results shown in Figure 8.

If the reverberation room is excited by ten uncorrelated sound sources, the dependency of the eigenvalue levels on sample length is largely reduced compared to the previous case with only one sound source. The results are shown in Figure 7 (bottom). However, the characteristics of an ideal diffuse sound field are still not reached, which again is in accordance with the spatial coherence shown in Figure 2 (bottom right).

4.4 Control performance

For reasons of brevity, the absolute disturbance rejection in third-octave bands is not provided. Instead, the maximum reductions in third-octave-band power level (averaged over E_1 and E_2) serve as reference for the relative disturbance rejections shown in Figure 8. These are $\approx 20\,\mathrm{dB}$ (in the $160\,\mathrm{Hz}$ third-octave band) for the generic double panel (simulation), $\approx 12\,\mathrm{dB}$ (in the $400\,\mathrm{Hz}$ third-octave band) for the real system with one sound source in the reverberation room, and $\approx 10\,\mathrm{dB}$ (in the $315\,\mathrm{Hz}$ third-octave band) for the real system with ten independent sound sources in the reverberation room.

As expected from the previous results, the dependency of the simulated disturbance rejection on FIR-filter-length is negligible. The relative disturbance rejection shown in Figure 8 amounts to only $\approx 5\,\%$ of the dB-value of the maximum third-octave-band power reduction which is rather small compared to the experimental results with non-ideal diffuse sound fields. In the real case with one sound source in the reverberation room, a maximum relative disturbance rejection of $3.7\,\mathrm{dB}$ is observed. This difference is significant since it amounts

to $\approx 30\,\%$ of the dB-value of the maximum third-octave-band power reduction. It can further be deduced from Figure 8 that, in general, the largest improvements of the feedforward controller with long FIR filters occur for small numbers of reference sensors. Also in the real case with ten independent sound sources in the reverberation room, the achieved relative disturbance rejection of up to $\approx 2.7\,\mathrm{dB}$ is significant, since it amounts to $\approx 27\,\%$ of the dB-value of the maximum third-octave-band power reduction. In contrast to the real case with one sound source in the reverberation room, the largest improvements in relative disturbance rejection occur here for higher numbers of reference sensors. This is due to the fact that, compared to the previous case, the number of dominant virtual noise sources has increased but still lies below the number of dominant virtual noise sources of an ideal diffuse field (see Figure 7 (bottom)). It can be assumed that, if the diffuse sound field was excited by a greater number of independent noise sources (leading to a better approximation of the ideal diffuse sound field), the relative disturbance rejection would decrease for seven and ten reference sensors as well and its dependency on the FIR-filter-length would vanish.

5 Conclusion

An expression for the spatial coherence of an ideal diffuse sound field is derived. It is used for the validation of an ideal pure-tone diffuse sound field simulation model and for the evaluation of the spatial coherence of real, non-ideal diffuse sound fields generated in reverberation rooms. Whereas the pure-tone diffuse sound field simulation model approximates the ideal diffuse sound field very well, deviations from the ideal case are observed for the real diffuse sound fields. It is emphasised that the quality of a real diffuse sound field, which is defined according to its closeness of agreement to the ideal case, not only depends on the reverberation room's Schröder frequency but also on the number of statistically independent sound sources exciting the reverberation room. The dependency of the spatial coherence on the duration of the measured signals is explained by the reverberation time. If the sample length is small compared to the reverberation time, the spatial coherence of a non-ideal diffuse sound field converges to the ideal case. This has implications on the performance of active feedforward control, since the number of filter weights, and hence the sample length the filter uses for correlation, is a free design parameter. So, in the case of a non-ideal diffuse sound field excitation, the mutual coherence between reference sensors and the multiple coherence between reference and error sensors will depend on the chosen filter length. Therefore, the optimal number and position of reference sensors cannot be chosen independently from the control filter length. Furthermore, the control performance might be overestimated compared to the ideal case. This leads to the conclusion that the suitability of reverberation rooms used as disturbance excitation for the evaluation of active structures with feedforward controllers is limited. Depending on the application scenario of the test specimen, the diffuse sound field needs to be excited by a sufficient number of independent noise sources. Alternatively, a more realistic acoustic excitation might be achieved by means of a loudspeaker array placed in front of the structure.

References

[1] M. Akiho, M. Haseyama, H. Kitajima, *Virtual reference signals for active noise cancellation system*, The Journal of the Acoustical Society of Japan (E), Vol. 19, No. 2, Acoustical Society of Japan (1998), pp. 95–103.

[2] C. Bao, J. Pan, *Experimental study of different approaches for active control of sound transmission through double walls*, The Journal of the Acoustical Society of America, Vol. 102, No. 3, Acoustical Society of America (1997), pp. 1664–1670.

[3] P. De Fonseca, P. Sas, H. Van Brussel, *Experimental study of the active sound transmission reduction through a double panel test section*, Acta Acustica united with Acustica, Vol. 85, No. 4, S. Hirzel Verlag (1999) pp. 538–546.

[4] S. J. Elliott, *Signal Processing for Active Control*, Academic Press, London (2001).

[5] S. J. Elliott, C. Maury, P. Gardonio, *The synthesis of spatially correlated random pressure fields*, The Journal of the Acoustical Society of America, Vol. 117, No. 3, Acoustical Society of America (2005), pp. 1186–1201.

[6] W. P. Engels, O. N. Baumann, S. J. Elliott, R. Fraanje, *Centralized and decentralized control of structural vibration and sound radiation*, The Journal of the Acoustical Society of America, Vol. 119, No. 3, Acoustical Society of America (2006), pp. 1487–1495.

[7] F. Fahy, P. Gardonio, *Sound and Structural Vibration: Radiation, Transmission and Response*, Academic Press, Oxford/Burlington, 2nd edition, (2007).

[8] P. Gardonio, N. Alujević, *Double panel with skyhook active damping control units for control of sound radiation*, The Journal of the Acoustical Society of America, Vol. 128, No. 3, Acoustical Society of America (2010), pp. 1108–1117.

[9] P. Gardonio, S. J. Elliott, *Active control of structure-borne and airborne sound transmission through double panel*, Journal of Aircraft, Vol. 36, No. 6, American Institute of Aeronautics and Astronautics (1999), pp. 1023–1032.

[10] P. Gardonio, S. J. Elliott, *Smart panels for active structural acoustic control*, Smart Materials and Structures, Vol. 13, No. 6, IOP Publishing UK (2004), pp. 1314–1336.

[11] T. Haase, S. Algermissen, O. Unruh, M. Misol, *Experiments on active control of counter-rotating open rotor interior noise*, Acta Acustica united with Acustica, Vol. 100, S. Hirzel Verlag (2014), pp. 448–457.

[12] F. Jacobsen, T. Roisin. *The coherence of reverberant sound fields*, The Journal of the Acoustical Society of America, Vol. 108, No. 1, Acoustical Society of America (2000), pp. 204–210.

[13] J. Minkoff, *The operation of multichannel feedforward adaptive systems*, IEEE Transactions on Signal Processing, Vol. 45, No. 12, Institute of Electrical and Electronics Engineers (1997), pp. 2993–3005.

[14] M. Misol, C. Bloch, H. P. Monner, M. Sinapius, *Performance of active feedforward control systems in non-ideal, synthesized diffuse sound fields*, The Journal of the Acoustical Society of America, Vol. 135, No. 4, Acoustical Society of America (2014), pp. 1887–1897.

[15] M. Misol, T. Haase, H. P. Monner, M. Sinapius, *Active trim panel with improved sound transmission loss under stochastic acoustic excitation*, in M. J. Crocker, M. Pawelczyk, B. Paosawatyanyong, editors, *Proceedings of the 20th International Congress on Sound and Vibration, Bangkok, Thailand, 2013 July 7–11*, Auburn AL USA (2013), CD-Rom.

[16] M. Misol, C. Hesse, *Numerische und experimentelle untersuchungen zur optimierung der sensorik von adaptiven steuerungen an doppelwandigen leichtbaustrukturen* DLR-IB 131-2012/43 (internal report), Deutsches Zentrum für Luft- und Raumfahrt e.V., Köln (2012), Germany.

[17] J. Pan, C. Bao, *Analytical study of different approaches for active control of sound transmission through double walls* The Journal of the Acoustical Society of America, Vol. 103, No. 4, Acoustical Society of America (1998), pp. 1916–1922.

[18] G. K. F. Rabl, *Recursive solution to wiener's multi-channel time filtering*, Astronomy & Astrophysics, Vol. 270, EDP Sciences (1993), pp. 552–556.

[19] M. Schröder, *Die statistischen parameter der frequenzkurven von großen räumen*, Acustica, Vol. 4, No. 2, S. Hirzel Verlag (1954), pp. 594–600.